



Coseismic fault slip of the 2008 M_w 7.9 Wenchuan earthquake estimated from InSAR and GPS measurements

GuangCai Feng,¹ Eric A. Hetland,² XiaoLi Ding,¹ ZhiWei Li,³ and Lei Zhang¹

Received 5 October 2009; revised 13 November 2009; accepted 23 November 2009; published 5 January 2010.

[1] We infer co-seismic fault slip during the 2008 M_w 7.9 Wenchuan earthquake from interferometric synthetic aperture radar (InSAR) and GPS observations of ground deformation. We use ALOS/PALSAR data from ascending orbits on six tracks, and we do not use data that are strongly affected by ionospheric perturbations. We use a fault model composed of three planar fault segments of the Beichuan fault, and one planar segment representing the parallel Pengguan fault. Maximum thrust-slip is up to 6.7 m near the surface, and occurs in two locations, near Yingxiu in the south and Beichuan in the center of the rupture. Maximum strike-slip is over 4 m, and occurs near Pingtong and Nanba along the northern end of the rupture. We find that the ratio of coseismic thrust- to strike-slip on the Beichuan fault decreases from 1.5 to 0.7 from the SW to the NE. **Citation:** Feng, G., E. A. Hetland, X. Ding, Z. Li, and L. Zhang (2010), Coseismic fault slip of the 2008 M_w 7.9 Wenchuan earthquake estimated from InSAR and GPS measurements, *Geophys. Res. Lett.*, 37, L01302, doi:10.1029/2009GL041213.

1. Introduction

[2] On 12 May 2008, the M_w 7.9 Wenchuan earthquake ruptured the middle segment of the Longmenshan (LMS) thrust belt, at eastern margin of the Tibetan Plateau [Burchfiel *et al.*, 2008]. The earthquake caused significant damage to Wenchuan, Beichuan, and Qingchuan Counties, resulting in tens of thousands of deaths. The Wenchuan earthquake also caused several landslides in the region, temporarily damming several rivers, which exacerbated the damage of the earthquake and severely complicated rescue efforts.

[3] Finite source inversion of seismic data indicates that the rupture initiated in the southwest of LMS fault zone and propagated toward the northeast along a SW–NE striking fault [Ji *et al.*, 2008]. The slip-model of Ji *et al.* [2008] assumed a single planar fault, dipping 33 deg. to the NW, and showed that the rupture was composed of two main sub-events, with a greater strike-slip component in the NE subevent. Coseismic fault scarps reveal a complicated pattern of slip, with the Wenchuan earthquake rupturing ~240 km of the Beichuan fault and ~72 km of the parallel Pengguan fault [Liu *et al.*, 2009; Lin *et al.*, 2009; Xu *et al.*, 2009]. Finally, analysis of aftershock locations indicates that the Beichuan section of the rupture is roughly composed of

two sections of similar length and different dip [Huang *et al.*, 2008; Xu *et al.*, 2009].

[4] In this study, we estimate the spatial pattern of coseismic slip on simplified geometries of the Beichuan and Pengguan faults from interferometric synthetic aperture radar (InSAR) and GPS measurements of coseismic surface deformation.

2. Data Processing

[5] We use L-band ALOS/PALSAR data from six ascending tracks 471 to 476 (Table 1), to form interferograms of coseismic deformation in regions that cover the LMS fault zone and the rupture of the Wenchuan earthquake (Figure 1a). L-band SAR has the advantage that it experiences less temporal decorrelation in heavily vegetated areas due to its ability to penetrate vegetation [Sandwell *et al.*, 2008]. The ALOS/PALSAR radar incidence angle is approximately 38.7° from vertical, so the measurements are slightly more sensitive to horizontal ground displacement than either ERS or ENVISAT, which have ~23° incidence. We process the SAR data from a level-1.0 product using the software package GAMMA [Wegmüller and Werner, 1997]. To remove effects of topography, we use a mosaic of Shuttle Radar Topography Mission digital elevation models with 90-m postings. Many of the acquisitions after the Wenchuan earthquake were affected by ionospheric perturbations, which G. C. Feng *et al.* (Ionospheric variation associated with Wenchuan M_w 8.0 earthquake observed with ALOS PALSAR, submitted to *Journal of Geophysical Research*, 2009) identified using the method proposed by Wegmüller *et al.* [2006] and Meyer *et al.* [2006]. We use the “ionosphere free” acquisitions proposed by Feng *et al.* (submitted manuscript, 2009) to determine interferograms of the coseismic deformation in the satellite line of sight (LOS) direction (Table 1 and Figure 1a). Feng *et al.* (submitted manuscript, 2009) did not find suitable ionosphere free acquisitions for track 475, so our interferogram for track 475 still contains a component of ionospheric contamination. The interferometric phase is measured modulo 2π and needs to be integrated (i.e., unwrapped) to determine relative LOS displacements, which we did using the branch-cut algorithm of Rosen *et al.* [1994]. The interferograms from tracks 473, 474, and 475 are discontinuous across the surface rupture, and thus we unwrap the hanging wall and footwall pieces of these interferograms separately.

[6] In addition to the LOS displacement, we calculated the offsets of pixels in the azimuth and range directions of the satellite geometry using the method of Strozzi *et al.* [2002] (auxiliary material).⁴ We use these pixel offsets

¹Department of Land Surveying and Geo-Informatics, Hong Kong Polytechnic University, Kowloon, Hong Kong.

²Department of Geological Sciences, University of Michigan, Ann Arbor, Michigan, USA.

³Department of Geomatics, Central South University, Changsha, China.

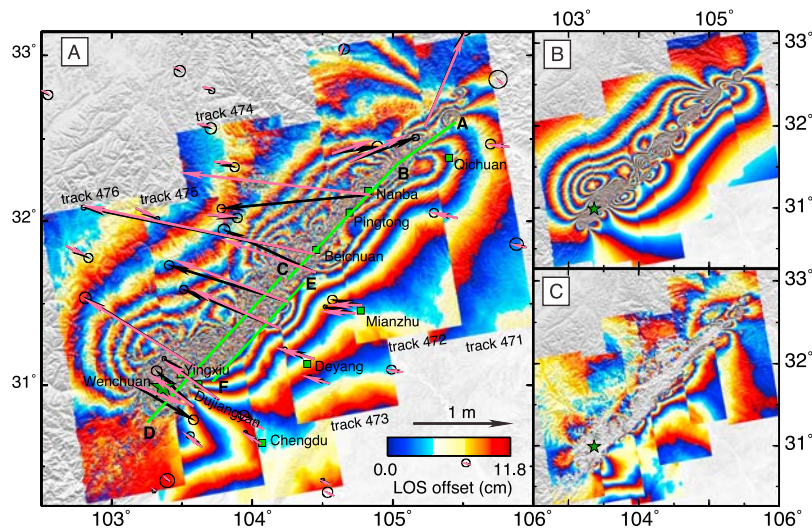


Figure 1. (a) InSAR and GPS observations of coseismic ground deformation; interferograms are shown without masking decorrelated regions, and GPS observations are shown by black vectors (ellipses denote the GPS uncertainties [from Zhang, 2008]). Also shown are the horizontal surface offsets predicted by our slip model (pink vectors), the epicenter of the Wenchuan earthquake (green star), locations of nearby cities (green squares), and surface traces of the fault segments in our fault model (light green lines; A-D are Beichuan fault segments and F-E is the Pengguan fault segment). (b) Interferograms predicted by the slip model in Figure 2 and simulated using the actual satellite geometry of each track. (c) Residuals between the observed and simulated interferograms; decorrelated regions of the interferograms are masked out.

to constrain the traces of the fault segments that ruptured in the Wenchuan earthquake. Pixel offsets are occasionally used as additional constraints on coseismic fault slip [e.g., Jónsson *et al.*, 2002; Simons *et al.*, 2002], although in this study, we don't use the pixel offset measurements to directly constrain fault slip. We also use GPS measurements of the horizontal coseismic deformation from 44 continuous stations in the Crustal Movement Observation Network of China and 78 campaign stations [Zhang, 2008].

3. Data Inversion and Coseismic Slip Model

[7] We use both field observations of fault scarps [Liu *et al.*, 2009; Lin *et al.*, 2009; Xu *et al.*, 2009] and InSAR pixel offset measurements (see auxiliary material) [see also Kobayashi *et al.*, 2009] to construct a simplified geometry of the faults that ruptured in the Wenchuan earthquake (Figure 2). Our fault model is composed of 4 fault segments, each of which have constant trace and dip (see auxiliary material for segment details). The first three segments compose the SW–NE striking Beichuan fault, while the fourth segment corresponds to rupture on the Pengguan fault. We assume that the dip of each fault segment is the average dip of the mapped surface scarps and aftershock

locations. We take the dip of the northern two segments of the Beichuan fault to be 67 deg., and the dip of the southern segment of the Beichuan to be 47 deg., while the dip of the Pengguan fault segment is 35 deg. We take the base of the Beichuan fault segments to be at 30 km depth. We take the base of the Pengguan fault segment to be at 15 km depth, so that it merges with Beichuan fault at its base [Hubbard and Shaw, 2009]. We divide the Beichuan fault segments into cells that are 4 km along strike by 4 km in depth, and we divide the Pengguan fault segment into 3 km by 3 km cells. We construct the Green's functions of surface displacements using Okada [1985], assuming a Poisson ratio of 0.25.

[8] We down-sample the unwrapped interferograms based on the fringe rate and the spatial coherence of the interferogram, reducing the number of data points from several million to 2150. We treat all InSAR observations as independent with estimated uncertainty of 4.5 cm, assuming that the range precision of ALOS/PALSAR is 1.5 times worse than the estimated precision for ERS/ASAR [Sandwell *et al.*, 2008]. Two of the InSAR images have perpendicular baseline distances of about 400 m, and a 5 m topographic error will lead to about a 2 cm error in LOS. We include nine additional parameters in the inversion, which describe

Table 1. ALOS/PALSAR Images Used for Generating Interferograms of Coseismic Surface Deformation

Track	Date of Master Image Acquisition	Date of Slave Image Acquisition	Days Before Wenchuan Eq.	Days After Wenchuan Eq.	Perpendicular Baseline (m)
471	11 Jan 2007	01 Dec 2008	487	203	405
472	28 Jan 2007	02 Feb 2009	470	266	−282
473	30 Dec 2006	04 Jan 2009	499	237	408
474	05 Mar 2008	05 Jun 2008	68	24	285
475	20 Jun 2007	22 Jun 2008	327	41	27
476	04 Jan 2007	24 Nov 2008	494	196	344

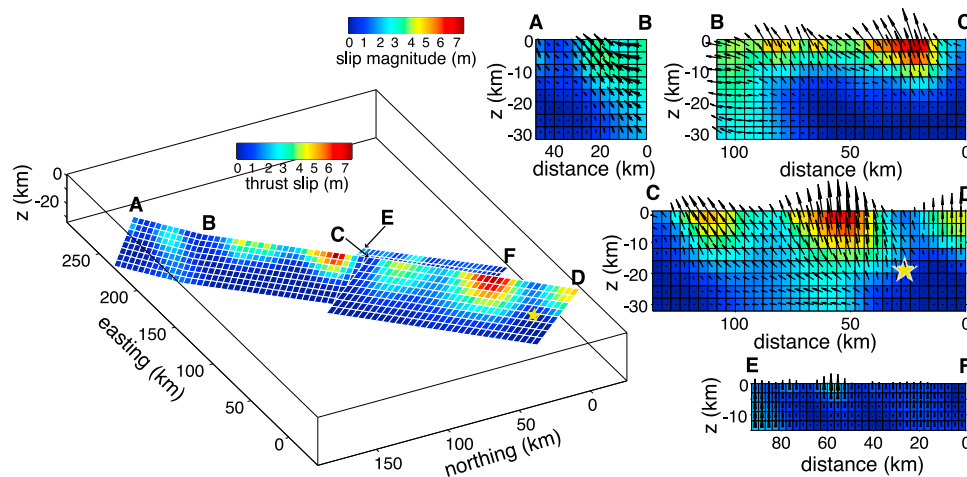


Figure 2. Distribution of coseismic fault slip from the joint inversion of the InSAR and GPS data. Colors in the 3D perspective plot indicate thrust-slip magnitude, and view is from the northwest. In the individual plots of the fault segments, color indicates the magnitude of the total fault slip, vectors indicate the direction of fault slip, and distance is relative to the start of each fault segment. Pale yellow star denotes the location of the hypocenter of the Wenchuan earthquake.

unknown offsets in the unwrapped interferograms. We use the formal errors for the GPS data [Zhang, 2008], and we weight the GPS nine times that of the InSAR observations. We apply an additional data weighting based on the distance of the observation from the fault traces, such that the farthest GPS observation at 270.5 km from the fault trace has half the weight of an observation the closest to the fault. This distance weighting results in far-field observations contributing slightly less to the coseismic slip, and slightly increases the fit to observations in the near field (where displacement gradients are large) and decreases the fit in the far-field (where displacement gradients are small). Due to our simplified fault model, the GPS station at Nanba is located on the incorrect side of our representation of the Beichuan fault. To correct this error, we perturbed the location of this GPS station 30 m to the SE, so that the GPS vector is correctly located on the foot-wall side of our fault model. We allow both thrust and right lateral strike-slip on the three Beichuan segments, and only allow thrust-slip on the Pengguan segment. The reason for the latter is the lack of mapped strike-slip fault scarps on the Pengguan fault. To avoid oscillations in the inferred fault slip during the inversion, we additionally minimize the Laplacian of the fault slip. We solve for fault slip on the four fault segments using nonnegative least squares [Lawson and Hanson, 1974], and determine the level of smoothing using Helmert variance component estimation [e.g., Sahin et al., 1992].

[9] The best-fit slip model predicts surface deformation similar to that observed, with a root mean square error to the GPS observations of 4.8 cm and 7.7 cm to the LOS observations (Figure 1). Our slip model shows thrust slip on all fault segments and variable right-lateral strike-slip on the three segments of the Beichuan fault (Figure 2). The total estimated moment magnitude is 7.9, assuming 34 GPa shear modulus. Thrust-slip is concentrated in the upper 15 km of the crust, with the largest thrust-slip of about 6.7 m near the epicenter and in the central part of the Beichuan fault. In contrast to the thrust-slip, the strike-slip tends to extend to deeper depths, although there is less resolution on the strike-slip component compared to the thrust-slip. The maximum

right-lateral slip is about 4.3 m on the Beichuan fault. There is less thrust-slip on the Pengguan fault segment, where maximum thrust-slip is 2.6 m. Our results indicate that the ratio of thrust- to strike-slip decreases from SW to NE along the Beichuan fault (Figure 2).

4. Discussion

[10] Our inferred coseismic slip model qualitatively agrees with the seismic finite source model of Ji et al. [2008], as well as coseismic slip models based on geodetic data [Hao et al., 2009; Hashimoto et al., 2009; Shen et al., 2009]. Surface offsets predicted from our slip model generally agree with mapped fault scarp offsets, although our predicted offsets on the Pengguan fault are on the low end of measurements [Liu et al., 2009; Lin et al., 2009; Xu et al., 2009] (auxiliary material). However, the surface offset measurements are quite noisy, and are not all from fault scarps that are oriented along the main trends of the Beichuan or Pengguan faults, and thus we do not use these data to score our final model. Finally, the locations of the largest fault offsets in our coseismic slip model correlate well with the near-field peak ground accelerations [Li et al., 2008; Wang and Xie, 2009].

[11] One of the most noteworthy features of the coseismic slip in the Wenchuan earthquake is that the amount of right-lateral fault slip on the Beichuan fault increases, and the thrust-slip decreases, from SW to NE. The total thrust-slip potency (slip times area) of the southernmost segment of the Beichuan fault is almost $10 \times 10^3 \text{ km}^2\text{m}$, while the potency of strike-slip is $6.8 \times 10^3 \text{ km}^2\text{m}$. On the other hand, the total thrust-slip potency on the two northern segments of the Beichuan fault is $5.5 \times 10^3 \text{ km}^2\text{m}$, and strike-slip potency is $8.2 \times 10^3 \text{ km}^2\text{m}$. The ratio of the thrust-slip to strike-slip potency on the southernmost segment is ~ 1.5 , as opposed to ~ 0.7 on both of the two northern segments. That thrust decreases, and strike-slip increases to the NE is consistent with other geodetic coseismic slip models [Hao et al., 2009; Hashimoto et al., 2009; Shen et al., 2009], although it conflicts with the interseismic strain accumulation model of

Burchfiel *et al.* [2008]. Using an interseismic block model, Burchfiel *et al.* [2008] infer a 1:1 ratio between thrust and right-lateral strain accumulation near the Wenchuan epicenter, whereas they infer a 3:1 ratio between thrust and right-lateral strain accumulation on the NE section of the fault.

[12] We note that with these data, our resolution of the strike-slip component of fault slip is poor compared to the thrust-slip resolution. This lack of resolution is mainly due to the fact that the LOS observations are more sensitive to vertical offsets compared to horizontal offsets, and there are relatively few GPS observations. Nevertheless, tests we have done indicate that the general pattern of increasing right-lateral slip to the NE is required by these data. The increase in strike-slip motion to the NE cannot be the result of a change in fault strike, and so may indicate that the stress-field is laterally heterogeneous. Indeed focal mechanisms of large aftershocks indicate that the stress field is heterogeneous [Wang and Xie, 2009], although it is not clear if these aftershocks reflect the stress field prior to the earthquake, or if they reflect the coseismic stress changes. It is interesting to note that there is more strike-slip motion on the steeper dipping Beichuan fault segments than on the more shallowly dipping segment to the SW.

[13] The amount of slip resolved on the Pengguan fault segment is small compared to the adjacent Beichuan fault. Additionally, the predicted surface offsets from our slip model of the Pengguan fault are on the low range of the field observations [Liu *et al.*, 2009; Lin *et al.*, 2009; Xu *et al.*, 2009] (auxiliary material). It may be that thrust slip on the Pengguan is being mapped onto the parallel Beichuan fault during inversion. As our interferograms are largely decorrelated between these faults, we are not able to uniquely attribute slip to either of these parallel faults. We also infer some thrust-slip on the SW edge of the Beichuan fault model. We believe that the slip in this region is poorly constrained with these data, especially at shallow depths, primarily due to InSAR decorrelation along the fault and few GPS sites at the SW end of the Wenchuan rupture (Figure 2). However, far-field LOS observations seem to require some thrust slip SW of the epicenter. The InSAR pixel offset measurements may be able to better constrain the partitioning of coseismic slip between the Beichuan and Pengguan faults, as well as at the SW edge of the Beichuan fault; although, we note that the uncertainty on the pixel offset measurements is generally larger than the data we use here.

[14] Aftershock locations and observations of fault scarps both indicate that the dip of Beichuan fault is steeper to the NE [Huang *et al.*, 2008; Xu *et al.*, 2009]. The fault model we consider in this paper is relatively simple, with an abrupt change in the dip of the Beichuan fault near the NE end of the Pengguan fault. In reality, the change in dip of the Beichuan fault may be smoother, and a more continuous representation of the Beichuan fault may yield a better fit to the data. The fault model of Shen *et al.* [2009] represented the Beichuan fault with 11 segments and included a more complex variation of fault dip. Our slip results are quite similar to those of Shen *et al.* [2009], although their results are much smoother, and it may be that differences between our models are due primarily to the inversion process and not fault geometry. We have also ignored any possible change in fault dip with depth. Hubbard and Shaw [2009]

infer a shallowing of fault dip below about 10 km depth at the SW end of the Beichuan fault, although most of our inferred coseismic fault slip is in the upper 10–15 km of the fault. Additionally, the left-lateral Xiaoyudong fault which trends NW–SE between the Beichuan and Pengguan faults, may have also slipped during the Wenchuan earthquake [Liu *et al.*, 2009; Lin *et al.*, 2009; Xu *et al.*, 2009].

[15] Due to ionospheric contamination of ALOS/PALSAR acquisitions after the Wenchuan earthquake (Feng *et al.*, submitted manuscript, 2009), only interferograms with large time span are used. These interferograms may contain ground deformation due to postseismic processes, including surface deformation from large aftershocks. Extrapolation of continuous GPS sites presented by Shen *et al.* [2009] indicate that postseismic surface offsets may be as much as 10% of the coseismic offsets over the first year following the earthquake. This value is location specific, and reflects the largest potential postseismic contribution at the continuous GPS sites. Our geodetic moment magnitude of 7.9 is larger than the 7.79 in the coseismic slip model of Hashimoto *et al.* [2009], which may be due to more postseismic fault slip in our model. The residual interferograms also show un-modeled near-field processes (Figure 1c) and there is a large misfit to the GPS observation near Nanba (Figure 1a); these misfits could be due to geometric complexity or postseismic process that are unaccounted for in our model.

5. Conclusions

[16] We use ALOS/PALSAR and GPS measurements of coseismic deformation from the 2008 Wenchuan earthquake to constrain fault slip on the Beichuan and Pengguan faults. We use a relatively simplified fault model, where we approximate the SW–NE striking, NW dipping Beichuan fault with three segments, with the southernmost segment more shallowly dipping than the northern two segments. We find that the amount of thrust-slip decreases to the NE along the Beichuan fault, and that the strike-slip increases to the NE. Hence, thrust-slip dominates the southernmost region of the Beichuan fault near the hypocenter, with right-lateral slip dominating to the NE. We also find that there is a small amount of thrust-slip on the parallel, and shallower dipping Pengguan fault to the SE of the Beichuan. Thrust-slip is concentrated in several regions of the fault, with maximum slip of almost 7 m at shallow depths near Yingxiu and Beichuan counties, while the largest strike-slip offsets (over 4 m) are located near Pingtong and Nanba counties.

[17] **Acknowledgments.** We thank the editor R. Harris and two anonymous reviewers for comments and suggestions. The ALOS/PALSAR data were provided by the Japan Aerospace Exploration Agency under Project AO-430. Inverse calculations were done using Matlab, The Mathworks Inc., and Figures 1 and 2 were produced using GMT [Wessel and Smith, 1998]. This research was conducted during a collaborative visit by G. Feng to the University of Michigan, funded by the Research Scholar Attachment Programme of the Hong Kong Polytechnic University (HKPU), with additional funding provided by an HKPU scholarship to G. Feng.

References

- Burchfiel, B. C., L. H. Royden, R. D. van der Hilst, B. H. Hager, Z. Chen, R. W. King, C. Li, J. Lü, H. Yao, and E. Kirby (2008), A geological and geophysical context for the Wenchuan earthquake of 12 May 2008, Sichuan, People's Republic of China, *GSA Today*, 18(7), 4–11, doi:10.1130/GSATG18A.1.

- Hao, K. X., H. Si, H. Fujiwara, and T. Ozawa (2009), Coseismic surface ruptures and crustal deformations of the 2008 Wenchuan earthquake $M_w7.9$, China, *Geophys. Res. Lett.*, *36*, L11303, doi:10.1029/2009GL037971.
- Hashimoto, M., M. Enomoto, and Y. Fukushima (2009), Coseismic deformation from the 2008 Wenchuan, China, earthquake derived from ALOS/PALSAR images, *Tectonophysics*, doi:10.1016/j.tecto.2009.08.034, in press.
- Huang, Y., J. P. Wu, T. Z. Zhang, and D. N. Zhang (2008), Relocation of the $M8.0$ Wenchuan earthquake and its aftershock sequence, *Sci. China Ser. D*, *51*(12), 1703–1711, doi:10.1007/s11430-008-0135-z.
- Hubbard, J., and J. H. Shaw (2009), Uplift of the Longmen Shan and Tibetan Plateau, and the 2008 Wenchuan ($M=7.9$) earthquake, *Nature*, *458*, 194–197, doi:10.1038/nature07837.
- Ji, C., G. Shao, Z. Lu, K. Hudnut, J. Jiu, G. Hayes, and Y. Zeng (2008), Rupture history of 2008 May 12 M_w 8.0 Wen-Chuan earthquake: Evidence of slip interaction, *Eos Trans. AGU*, *89*(53), Fall Meet. Suppl., Abstract S23E–02.
- Jónsson, S., H. Zebker, P. Segall, and F. Amelung (2002), Fault slip distribution of the 1999 $M7.2$ Hector Mine earthquake, California, estimated from satellite radar and GPS measurements, *Bull. Seismol. Soc. Am.*, *92*(4), 1377–1389, doi:10.1785/0120000922.
- Kobayashi, T., Y. Takada, M. Furuya, and M. Murakami (2009), Locations and types of ruptures involved in the 2008 Sichuan earthquake inferred from SAR image matching, *Geophys. Res. Lett.*, *36*, L07302, doi:10.1029/2008GL036907.
- Lawson, C. L., and R. J. Hanson (1974), *Solving Least Squares Problems*, Prentice-Hall, Englewood Cliffs, N. J.
- Li, X., Z. Zhou, H. Yu, R. Wen, D. Lu, M. Huang, Y. Zhou, and J. Cu (2008), Strong motion observations and recordings from the great Wenchuan earthquake, *Earthquake Eng. Eng. Vib.*, *7*, 235–246, doi:10.1007/s11803-008-0892-x.
- Lin, A., Z. Ren, D. Jia, and X. Wu (2009), Co-seismic thrusting rupture and slip distribution produced by the 2008 M_w 7.9 Wenchuan earthquake, China, *Tectonophysics*, *471*, 203–215.
- Liu, Z., et al. (2009), Co-seismic ruptures of the 12 May 2008, M_s 8.0 Wenchuan earthquake, Sichuan: East-west crustal shortening on oblique, parallel thrusts along the eastern edge of Tibet, *Earth Planet. Sci. Lett.*, *286*, 355–370, doi:10.1016/j.epsl.2009.07.017.
- Meyer, F., R. Bamler, N. Jakowski, and T. Fritz (2006), The potential of low-frequency SAR systems for mapping ionospheric TEC distributions, *IEEE Geosci. Remote Sens. Lett.*, *3*(4), 560–564, doi:10.1109/LGRS.2006.882148.
- Okada, Y. (1985), Surface deformation due to shear and tensile faults in a half-space, *Bull. Seismol. Soc. Am.*, *75*(4), 1135–1154.
- Rosen, P. A., A. Hiramatsu, and C. L. Werner (1994), Two-dimensional phase unwrapping of SAR interferograms by charge connection through neutral trees, paper presented at International Geoscience and Remote Sensing Symposium, 1994, Jet Propul. Lab., Pasadena, Calif.
- Sahin, M., P. A. Cross, and P. C. Sellers (1992), Variance component estimation applied to satellite laser ranging, *Bull. Geod.*, *66*, 284–295, doi:10.1007/BF02033189.
- Sandwell, D. T., D. Myer, R. Mellors, M. Shimada, B. Brooks, and J. Foster (2008), Accuracy and resolution of ALOS interferometry: Vector deformation maps of the Father's Day intrusion at Kilauea, *IEEE Trans. Geosci. Remote Sens.*, *46*(11), 3524–3534, doi:10.1109/TGRS.2008.2000634.
- Shen, Z. K., J. B. Sun, P. Z. Zhang, Y. G. Wan, M. Wang, R. Bürgmann, Y. H. Zeng, W. J. Gan, H. Liao, and Q. L. Wang (2009), Slip maxima at fault junctions and rupturing of barriers during the 2008 Wenchuan earthquake, *Nature Geosci.*, *2*, 718–724, doi:10.1028/NGE0636.
- Simons, M., Y. Fialko, and L. Rivera (2002), Coseismic deformation from the 1999 M_w 7.1 Hector Mine, California, earthquake as inferred from InSAR and GPS observations, *Bull. Seismol. Soc. Am.*, *92*(4), 1390–1402, doi:10.1785/0120000933.
- Strozzi, T., A. Luckman, T. Murray, U. Wegmüller, and C. L. Werner (2002), Glacier motion estimation using SAR offset-tracking procedures, *IEEE Trans. Geosci. Remote Sens.*, *40*(11), 2384–2391, doi:10.1109/TGRS.2002.805079.
- Wang, D., and L. Xie (2009), Attenuation of peak ground accelerations from the great Wenchuan earthquake, *Earthquake Eng. Eng. Vib.*, *8*, 179–188, doi:10.1007/s11803-009-8139-z.
- Wegmüller, U., and C. L. Werner (1997), Gamma SAR processor and interferometry software, *Eur. Space Agency Spec. Publ.*, *414*, 1686–1692.
- Wegmüller, U., C. L. Werner, T. Strozzi, and A. Wiesmann (2006), Ionospheric electron concentration effects on SAR and InSAR, in *IGARSS 2006: IEEE International Conference on Geoscience and Remote Sensing Symposium, 2006*, pp. 3714–3717, Inst. of Electr. and Electr Eng, New York.
- Wessel, P., and W. H. F. Smith (1998), New, improved version of the Generic Mapping Tools released, *Eos Trans. AGU*, *79*(47), 579, doi:10.1029/98EO00426.
- Xu, X. W., X. Wen, G. Yu, G. Chen, Y. Klinger, J. Hubbard, and J. Shaw (2009), Co-seismic reverse-and oblique-slip surface faulting generated by the 2008 $M_w7.9$ Wenchuan earthquake, China, *Geology*, *37*(6), 515–518, doi:10.1130/G25462A.1.
- Zhang, P. Z. (2008), The co-seismic surface displacement of the great Wenchuan earthquake of May 12, 2008, Sichuan, China, from GPS measurements (in Chinese), *Chin. Sci.*, *38*(10), 1195–1206.
- X. Ding, G. Feng, and L. Zhang, Department of Land Surveying and Geo-Informatics, Hong Kong Polytechnic University, Kowloon, Hong Kong.
- E. A. Hetland, Department of Geological Sciences, University of Michigan, Ann Arbor, MI 48109, USA. (ehetland@alum.mit.edu)
- Z. Li, Department of Geomatics, Central South University, Changsha 410083, China.